

## Tailoring the FeO/SiO<sub>2</sub> ratio in electric arc furnace slags to minimize the leaching of vanadium and chromium




Simone Neuhold, David Algermissen, Peter Drissen, Burkart Adamczyk, Peter Presoly, Klaus P. Sedlazeck, Johannes Schenk, Johann G. Raith, Roland Pomberger, Daniel Vollprecht

### Angaben zur Veröffentlichung / Publication details:

Neuhold, Simone, David Algermissen, Peter Drissen, Burkart Adamczyk, Peter Presoly, Klaus P. Sedlazeck, Johannes Schenk, Johann G. Raith, Roland Pomberger, and Daniel Vollprecht. 2020. "Tailoring the FeO/SiO<sub>2</sub> ratio in electric arc furnace slags to minimize the leaching of vanadium and chromium." *Applied Sciences* 10 (7): 2549.  
<https://doi.org/10.3390/app10072549>.

## Article

# Tailoring the FeO/SiO<sub>2</sub> Ratio in Electric Arc Furnace Slags to Minimize the Leaching of Vanadium and Chromium

Simone Neuhold <sup>1,\*</sup>, David Algermissen <sup>2</sup>, Peter Drissen <sup>2</sup>, Burkart Adamczyk <sup>3</sup>, Peter Presoly <sup>4</sup>, Klaus P. Sedlazeck <sup>1</sup>, Johannes Schenk <sup>4</sup>, Johann G. Raith <sup>5</sup>, Roland Pomberger <sup>1</sup> and Daniel Vollprecht <sup>1</sup>

<sup>1</sup> Waste Processing Technology and Waste Management, Montanuniversitaet Leoben, Franz-Josef-Straße 18, 8700 Leoben, Austria; philipp.sedlazeck@unileoben.ac.at (K.P.S.); roland.pomberger@unileoben.ac.at (R.P.); daniel.vollprecht@unileoben.ac.at (D.V.)

<sup>2</sup> FEhS Building Materials Institute, Bliersheimer Straße 62, 47229 Duisburg, Germany; d.algermissen@fehs.de (D.A.); p.drissen@fehs.de (P.D.)

<sup>3</sup> Federal Institute for Materials Research and Testing, Richard-Willstätter-Straße 11, 12489 Berlin, Germany; burkart.adamczyk@bam.de

<sup>4</sup> Ferrous Metallurgy, Montanuniversitaet Leoben, Franz-Josef-Straße 18, 8700 Leoben, Austria; peter.presoly@unileoben.ac.at (P.P.); johannes.schenk@unileoben.ac.at (J.S.)

<sup>5</sup> Resource Mineralogy, Montanuniversitaet Leoben, Peter Tunner-Straße 5, 8700 Leoben, Austria; johann.raith@unileoben.ac.at

\* Correspondence: simone.neuhold@unileoben.ac.at

Received: 17 February 2020; Accepted: 3 April 2020; Published: 8 April 2020



**Abstract:** Based on recently published research on leaching control mechanisms in electric arc furnace (EAF) slags, it is assumed that a FeO/SiO<sub>2</sub> ratio of around one leads to low leached V and Cr concentrations. This ratio influences the mineral phase composition of the slag toward higher amounts of spinel and a lower solubility of calcium silicate phases by suppressing the formation of magnesiowuestite and highly soluble calcium silicate phases. To evaluate this hypothesis, laboratory and scaled up tests in an EAF pilot plant were performed on slag samples characterized by elevated V and Cr leaching and a high FeO/SiO<sub>2</sub> ratio. Prior to the melting experiments, the optimum FeO/SiO<sub>2</sub> ratio was calculated via FactSage<sup>TM</sup>. In the melting experiments, the ratio was adjusted by adding quartz sand, which also decreased the basicity (CaO/SiO<sub>2</sub>) of the slag. As a reference, remelting experiments without quartz sand addition were conducted and additionally, the influence of the cooling rate of the slag was examined. The remelted (without quartz sand) and the remelted modified slags (with quartz sand) were analyzed chemically and mineralogically and the leaching behavior was investigated. The modification of the slags yielded a minimized release of V and Cr, supporting the hypothesis that the FeO/SiO<sub>2</sub> ratio influences the mineralogy and the leaching behavior.

**Keywords:** electric arc furnace (EAF) slags; FactSage<sup>TM</sup> calculations; leaching control mechanisms; melting experiments; quartz sand

## 1. Introduction

Various studies on the influence of the chemical and mineralogical composition on the release of heavy metals from steel slags as well as on surface reactions controlling the leaching behavior of slags are available (e.g., Aldrian et al. (2015), Cabrera-Real et al. (2012), Hobson et al. (2017), Loncnar et al. (2016), Mombelli et al. (2016), Mudersbach et al. (2009), Strandkvist et al. (2012), and van Zomeren et al. (2011) [1–8]). However, conclusions drawn from these studies are not always

applicable for all elements and all slag systems. Therefore, further investigations are required on the leaching control mechanisms of, for example, V in electric arc furnace (EAF) slags. In a previously conducted research [9], a mineralogical and chemical characterization of EAF slags was combined with a hydrogeochemical model and a hypothesis was proposed that the FeO/SiO<sub>2</sub> ratio in the slag is decisive for the amount of V and Cr released. It was assumed that a higher amount of FeO compared to SiO<sub>2</sub> leads to a higher abundance of wuestite (Fe, Mg, Mn)O and impedes the formation of Fe bearing calcium silicate phases such as olivine (A<sub>2</sub>SiO<sub>4</sub>, A = Ca, Mg, Mn, Fe) and melilite (Ca<sub>2</sub>M(XSiO<sub>7</sub>), M = Mg, Fe, Al and X = Si, Al) and also indirectly on the formation of spinel (AB<sub>2</sub>O<sub>4</sub>, A = Mg, Fe, Mn and B = Cr, Al, Fe, Mn). These previous investigations further showed that V and Cr were bound in spinel and wuestite; additionally, V was incorporated in larnite (β-Ca<sub>2</sub>SiO<sub>4</sub>) and Cr in olivine and/or melilite. It was also shown that olivine, enriched in Fe and Mn, spinel and melilite are less soluble than olivine (with comparable low Fe and Mn amount), wuestite, and larnite. In addition, it is assumed that hydrated Fe bearing calcium silicate phases may provide adsorption sites for V [9,10]. To minimize the V and Cr release, the formation of spinel must therefore be promoted and the formation of the highly soluble calcium silicate phases impeded. It is further assumed that the distribution and composition of the mineral phases can be tailored toward a reduced V and Cr release by a targeted adjustment of the chemical composition (i.e., the FeO/SiO<sub>2</sub> ratio).

A low leaching of potentially environmentally hazardous elements from steel slags is essential for the safe use of EAF slags as a substitution for natural aggregates (e.g., in road construction or concrete). The mechanical properties and the suitability of EAF slags as recycling building material are described by Faleschini et al. (2016), Pasetto and Baldo (2011) and Sas et al. (2015) [11–14]. Comparable mechanical properties between natural and industrial aggregates (i.e., magmatic rocks and steel slags) originate from similar formation processes with the two main differences being in SiO<sub>2</sub> and CaO concentrations or the basicity (CaO/SiO<sub>2</sub>) as well as the cooling rate. During the steel making process, slag forming components such as lime (CaO) and/or MgO-containing compounds (magnesite (MgCO<sub>3</sub>), dolomite (CaMg(CO<sub>3</sub>)<sub>2</sub>)) are added to form slag. Additionally, fluxes (e.g., fluorite (CaF<sub>2</sub>) or quartz (SiO<sub>2</sub>)) may be added to the slag to influence its viscosity [15,16]. Therefore, CaO concentrations in natural rocks (except limestone (CaCO<sub>3</sub>) and dolomite) are lower than in slags, whereas the SiO<sub>2</sub> concentrations are higher. Furthermore, while most natural igneous rocks solidify over long periods of time, steel slags cool down within one day, however, changing parameters during cooling such as melt composition (fractional crystallization) and oxygen potential, which also influence the phase composition and distribution in magmatic rocks, can be transferred to slag formation. This is also evident since mineral phases occurring in nature are also found in steel slags [17,18].

The potential of tailoring mechanical properties and leaching behavior of steel slags by adjusting the slag forming components and process parameters (cooling rate) is described, for example, by Cabrera-Real et al. (2012) and Tossavainen et al. (2007) [5,19]. The influence of quartz addition on the phase stability with respect to the hydraulic behavior was investigated by Mombelli et al. (2014) [20].

In this study, an optimized FeO/SiO<sub>2</sub> ratio in the molten slag was calculated with FactSage<sup>TM</sup> and evaluated with melting experiments in the laboratory and pilot plant scale. Additionally, different cooling rates were applied. After the experiments, the modification of the mineralogical phase distribution and leaching behavior was investigated. The results support the proposed hypothesis and may serve as a basis for further investigations toward an industrial application.

## 2. Materials and Methods

### 2.1. Sample Selection

For the laboratory experiments, a collective EAF slag sample (sample A) from a previous study [9] was used, which showed high FeO and low SiO<sub>2</sub> abundances and increased V and Cr leaching compared to the other samples investigated. The sampling was performed in 2016 and was assigned to the production of one steel charge during standard operating conditions. On the basis of ÖNORM S

2127 [21], ten subsamples of 36 kg, yielding a total amount of 360 kg, were taken. These samples were crushed (jaw crusher, Retsch BB 200) separately to <5 mm for the laboratory experiments and 350 g of the grain size fraction 1–5 mm of each sample were homogenized, forming sample A.

For the pilot scale experiments, the sampling was repeated in 2018 (sample B, approximately 700 kg). The sample again represented the standard procedure of the same steel plant, but with higher lime input compared to 2016. The samples were used as delivered, without further processing.

For comparison, this study also presented one EAF slag sample (sample C) from a second steel plant, which leached significantly lower amounts of V and Cr than sample A and was characterized by a FeO/SiO<sub>2</sub> ratio of approximately one [9].

## 2.2. Metallurgical Calculations

All calculations were performed using the software FactSage™ (version 7.1) in equilibrium mode selecting the databases FToxid (FACT oxide database, 2017) and FactPS (FACT pure substances database, 2017). Based on the mineralogical characterizations [9], it was decided that the six-component-system CaO–SiO<sub>2</sub>–FeO–MgO–Al<sub>2</sub>O<sub>3</sub>–Cr<sub>2</sub>O<sub>3</sub> served as a good compromise between a simplified slag system and all necessary components for the formation of the main mineral phases of samples A, B and C, namely: spinel solid solutions, wuestite solid solutions, and different calcium silicate phases such as melilite, larnite, and olivine.

In the first step, calculations were performed to compare the thermodynamic phase calculations with the experimental mineralogical results obtained. The chemical composition of the six components was normalized in proportion to their original amounts in the slag with their sum being 100 g. Phase formation was calculated in the temperature interval from 2000 °C to 500 °C with 50 °C steps and a pressure of 1 atm. Input data and selected base phases with end members are provided in the Supplementary Materials in Table S1.

Based on the results of the first set of calculations, a temperature was selected at which the experimentally determined mineralogical phase proportions and the calculated proportions for samples A and C were in good agreement. At this temperature, the second set of calculations was carried out, in which the amount of SiO<sub>2</sub> of sample A was varied from 0 g to 60 g in steps of 5 g. The chemical composition at which the mineralogical phase distribution changed to low amounts of wuestite and high amounts of calcium silicates and spinel was normalized to 100 g and the amount of SiO<sub>2</sub> required for the experiments was calculated taking into account the already present SiO<sub>2</sub> in the slag. Calculations for sample B were performed subsequently to the laboratory tests, using the same methodology as with sample A.

## 2.3. Melting Experiments

### 2.3.1. Laboratory Scale

The melting experiments were conducted at the FEhS Building Materials Institute in Duisburg using a Tammann furnace flushed with nitrogen. Two sets of experiments were executed: for the first set (experiments 1–3), sample A was solely remelted and cooled with three different cooling rates, yielding three samples (samples AR1–AR3); for the second set (experiments 4–6), the exact same procedure was applied, but sample A was mixed with SiO<sub>2</sub> prior to melting, yielding three additional samples (samples AC1–AC3).

For all experiments, MgO crucibles were used (manufactured at the FEhS Building Materials Institute). For experiments 1–3, the crucibles were filled with 2.6 g (1 mass-%) iron filings (ARMCO®, to additionally prevent an oxidation of the melt) and 260 g of slag sample A. The crucibles were placed in the furnace and heated with approximately 300 °C/h. Ten minutes after the sample had completely melted (1600 °C), the melt was poured onto a steel plate (experiment 1: fast cooling, sample AR1). The same procedure was repeated for experiment 2, but instead of pouring the melt on a steel plate, the sample was air-cooled in the crucible, simulating a moderate cooling rate (sample AR2). In experiment

3, the melt was cooled in the crucible in the furnace (the furnace was switched off), representing a slow cooling rate (sample AR3).

For experiments 4–6, 2.6 g (1 mass-%) iron filings (ARMCO®) and a mixture of 204 g of slag sample A and 56 g of SiO<sub>2</sub> (dried prior to the melting experiments) were placed into the crucible. The quartz sand used had a purity of 99.1% SiO<sub>2</sub> and no relevant impurities (e.g., V = 0.003 mg/L, Cr < 0.002 mg/L, according to DIN 19,529 [22]) were detected. The same procedure as in experiments 1–3 was applied, yielding samples AC1 (fast cooling), AC2 (moderate cooling), and AC3 (slow cooling).

### 2.3.2. Pilot Plant Scale

The melting experiments on a pilot plant scale were performed at the Federal Institute for Materials Research and Testing (BAM) in Berlin-Adlershof using a pilot plant scale EAF (alternating current, three graphite electrodes, 450 kVA apparent power, 150 kg/h throughput) with MgO bricks and MgO ramming mixture as the refractory material. Analogous to the laboratory tests, two series of experiments were carried out. For the first set (experiments 1–3), sample B was solely remelted and cooled with three different cooling rates, yielding three samples (samples BR1–BR3). For the second set (experiments 4–6), exactly the same procedure was applied but SiO<sub>2</sub> was added to the molten slag and homogenized by stirring (samples BC1–BC3). Sample B was dried in a drying oven (190 °C) before the experiments to avoid deflagrations in the furnace.

For experiments 1–3, 40 kg of sample B was provided in the furnace with iron filings (3.5 kg) on top and the arc was ignited. Additional 60 kg of sample B was added stepwise from 10 to 20 kg. After sample B had completely melted, the temperature was measured ( $T = 1735$  °C, temperature measuring lance) and approximately 20 kg of the melt was poured into a cast iron mold (air-cooled, moderate cooling rate, sample BR2). Afterward, another 20 kg of sample B was added to the furnace, melted ( $T = 1741$  °C), and approximately 10 kg of the melt was poured into a graphite mold embedded in a bed of corundum to achieve a very slow cooling (sample BR3). Subsequently, approximately 10 kg of the melt ( $T > 1800$  °C) was poured flat into a cast iron trough where it was cooled by stirring and simultaneously applying compressed air to simulate a fast cooling (sample BR1). After experiments 1–3, another 30 kg of sample B was added and melted in the furnace. By estimating the actual weights of the produced sample (via mold dimension, filling level, and density) and the residual melt in the furnace, the required amount of SiO<sub>2</sub> was calculated based on the conducted FactSage<sup>TM</sup> calculations (see Section 2.2). Twenty-nine kilograms of quartz sand (Weferlingen, WF03 [23]) was added stepwise to the melt. After the melt had been homogenized, rapid cooling (approximately 10 kg, sample BC1), slow cooling (approximately 16 kg, sample BC3), and moderate cooling (approximately 18 kg, sample BC2) was performed as described for experiments 1–3.

### 2.4. Sample Characterization

All samples (original samples and samples originating from the experiments) were characterized chemically and mineralogically and the leaching behavior was determined.

Prior to chemical characterization, the samples were crushed (jaw, crusher Retsch BB 200), ground (ball mill, Retsch S 1000), dried at  $105 \pm 3$  °C (drying oven, according to DIN EN 14346 [24]), and digested in a microwave with a mixture of HF, HNO<sub>3</sub>, and HCl, according to ÖNORM EN 13656 [25]. Leaching tests were performed in overhead shaker experiments with a grain size <1 mm, according to ÖNORM EN 14429 [26]. For the samples derived from the laboratory scale experiments, only leachates with distilled water (liquid:solid ratio = 10, 48 h) were prepared (two leachates per sample). For the samples from the pilot scale experiments, nine leachates (one with distilled water and eight with either HNO<sub>3</sub> or NaOH addition) were prepared to investigate the pH-dependent leaching behavior. The required amount of HNO<sub>3</sub> or NaOH was determined prior to the experiments via the acid and base neutralization capacity. The final pH values after 48 h ranged from pH 2 to 13. The pH was measured after 4 h, 44 h, and 48 h and the maximum pH change between 44 h and 48 h did not exceed 0.3 pH units. The digested samples and the leachates were analyzed at the Chair of Waste Processing



Technology and Waste Management of the Montanuniversitaet Leoben by using inductively coupled plasma mass spectrometry (ICP-MS, Agilent Type 7500), according to ÖNORM EN ISO 17294-2 [27].

The mineralogical bulk composition was analyzed by x-ray diffraction (XRD, PANalytical X'Pert Pro instrument) at the Institute of Applied Geosciences of the Graz University of Technology. The samples were rotated and data were collected for a  $2\theta$  angle between  $4^\circ$  and  $85^\circ$  with a step size of  $0.008^\circ$ , using Co-K $\alpha$  radiation at 40 mA and 45 kV.

Electron microprobe (EMP) analyses were performed with a Superprobe JEOL JXA 8200 at the Chair of Resource Mineralogy of the Montanuniversitaet Leoben. Quantitative element analyses and element mappings were recorded in wavelength dispersive spectrometer (WDS) mode using the K $\alpha$  lines of Ca, Mg, Mn, Si, Al, Fe, V, Cr, Mo, and F. The following spectrometer crystal arrangement was selected: TAP for Mg, Al, and F; PETJ for Si, Ca, and Mo; and LIFH for V, Cr, Mn, and Fe. The instrument was operated with an acceleration voltage of 15 kV and a beam current of 10 nA and calibrated with the following standards: chromite, chromium (III) oxide, wollastonite, diopside, and kaersutite. The detection limits are given separately for all measured elements and samples in Tables S2–S21.

### 3. Results and Discussion

#### 3.1. Comparison of Thermodynamic Calculations and Mineralogical Investigations

Comparison of the performed FactSage<sup>TM</sup> equilibrium calculations (Figure 1a–c) with the mineralogical analysis of the phase composition and phase distribution (Figure 2) revealed that the phase proportions for samples A and C were best reproduced at  $850^\circ\text{C}$ . Therefore, the influence of the quartz addition on the phase distribution and the amount of quartz sand required for the experiments was calculated at  $850^\circ\text{C}$  in equilibrium mode.

The calculations performed on sample A (laboratory experiments) and sample B (pilot scale experiments) at  $850^\circ\text{C}$  with varying SiO<sub>2</sub> content are shown in Figure 1a',b'. Above 35 g and 30 g SiO<sub>2</sub>, respectively, no wuestite (MeO\_A), moderate spinel (SPINA), and more calcium silicates (olivine (OlivA), melilite (Mel\_A), and clinopyroxene (cPyr;  $M_1M_2T_2O_6$ ,  $M_1 = \text{Ca, Mg, Fe, Mn}$  and  $M_2 = \text{Al, Mn, Mg, Fe}$  and  $T = \text{Si, Al, Fe}$ )) were formed. As it is assumed that melilites hydrate [10] and yield possible adsorption sites [9], the SiO<sub>2</sub> concentration corresponding to the highest melilite abundance (= 40 g SiO<sub>2</sub>) was chosen for the laboratory experiments (Figure 1), resulting in a normalized total SiO<sub>2</sub> content of 31.3 g. This changed the FeO/SiO<sub>2</sub> ratio from 3.66 to 1.12 and the CaO/SiO<sub>2</sub> ratio from above two (2.03) to below one (0.62). Taking into account the already present SiO<sub>2</sub>, the input for the laboratory experiments was 56 g quartz sand (assumption: SiO<sub>2</sub> purity = 100%) and 204 g of sample A. For the pilot scale experiments, the same calculations were performed for sample B, resulting in a calculated SiO<sub>2</sub> amount of 27.3 kg per 100 kg of sample B and a changed FeO/SiO<sub>2</sub> ratio from 3.42 to 1.06 and a CaO/SiO<sub>2</sub> ratio from 2.38 to 0.74.

Sample B (higher CaO input) could only be characterized chemically prior to the pilot scale experiments. Mineralogical examination afterward revealed that larnite and brownmillerite (Ca<sub>2</sub>(Al,Fe)<sub>2</sub>O<sub>5</sub>) were formed in sample B, instead of olivine and melilite (Figure 2a,b). The performed FactSage<sup>TM</sup> calculations (Figure 1b) showed that larnite (bC2SA) with 99.6% Ca<sub>2</sub>SiO<sub>4</sub> (0.4% Mg<sub>2</sub>SiO<sub>4</sub> and  $2.7 \cdot 10^{-02}\%$  Fe<sub>2</sub>SiO<sub>4</sub>) was formed at a transition temperature of  $865.7^\circ\text{C}$  and that therefore, the calculations for the pilot scale experiments were not performed at the optimum temperature. The implementation of brownmillerite (C2AF, not shown) resulted in low calculated concentrations of brownmillerite and melilite in both samples A and B, although no brownmillerite was identified experimentally in sample A and no melilite in sample B, respectively.

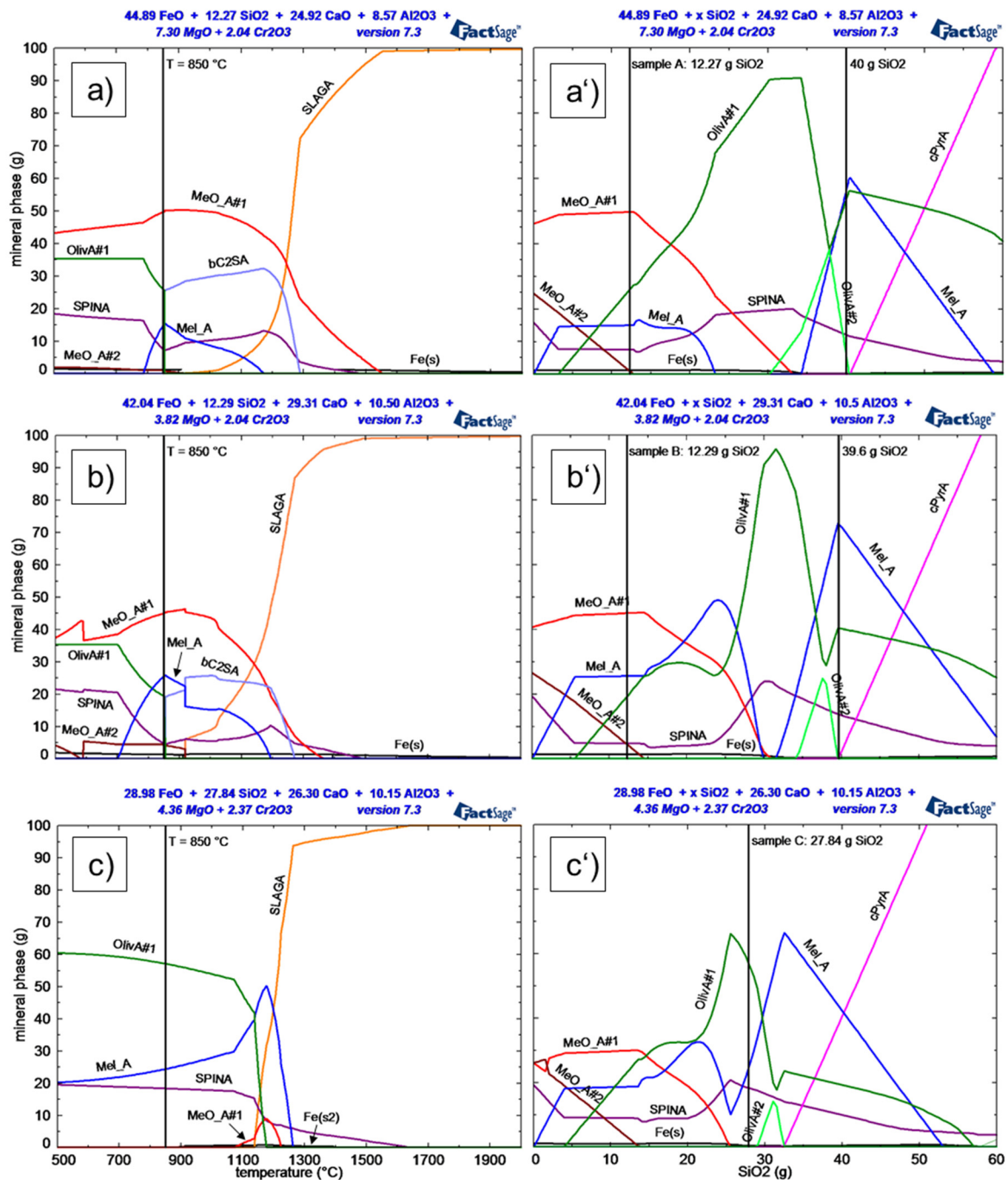


**Figure 1.** FactSage™ calculations. (a) and (a') sample A, (b) and (b') sample B and (c) and (c') sample C. (a–c) Mineral phase composition as a function of temperature. (a'–c') Mineral phase composition at 850 °C with varying SiO<sub>2</sub> content (not normalized); the normalized SiO<sub>2</sub> concentration of samples A–C as well as the target SiO<sub>2</sub> concentrations for samples A and B are marked. Abbreviations according to FactSage™: liquid slag (SLAGA), olivine group (OlivA), melilite group (Mel\_A), wuestite solid solution (MeO\_A), spinel solid solution (SPINA), clinopyroxene (cPyrA), larnite (bC2SA), and Fe(bcc) (Fe(s)). Plotted for publication with version 7.3 (FToxid, 2019 and FactPS, 2019) and calculated as described in Section 2.2.

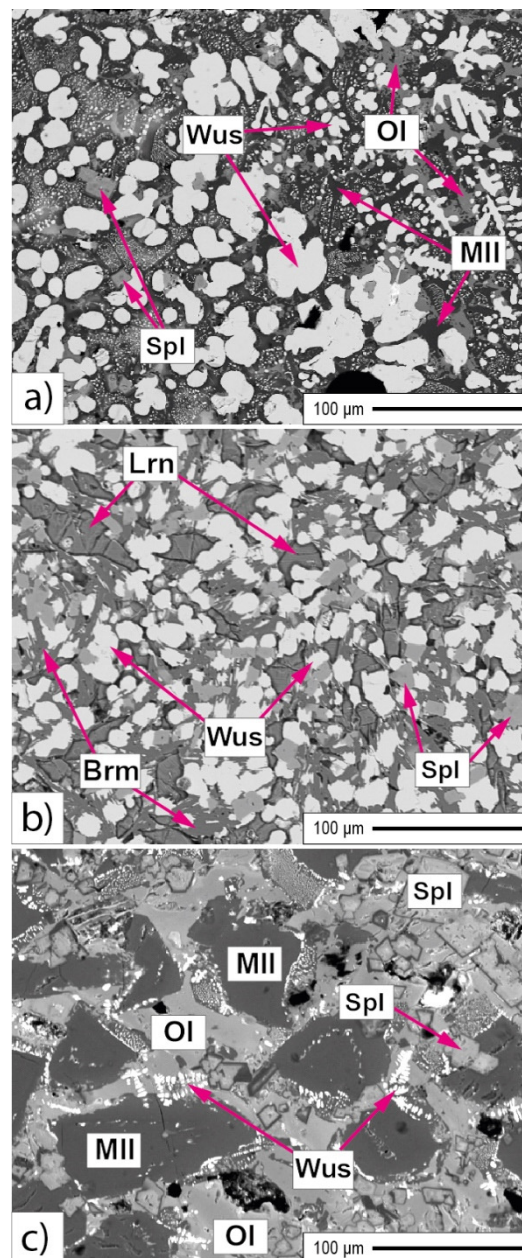


**Figure 2.** Back scattered electron (BSE) images. (a) Sample A, (b) Sample B, and (c) Sample C showing the main mineral phase composition derived from x-ray diffraction (XRD) and, if possible, electron microprobe (EMP) measurements. Abbreviations according to Whitney and Evans (2010) [28]: wuestite solid solution (Wus), spinel solid solution (Spl), larnite (Lrn), brownmillerite (Brm), olivine group (Ol), and melilite group (Mll).

### 3.2. Mineralogical Results of Laboratory and Pilot Scale Experiments

The mineralogy of the EAF slag samples after the experiments is shown in Figures 3 and 4 and Figure S1. In both cases (laboratory and pilot scale experiments), the results supported the FactSage<sup>TM</sup> calculations and the hypothesis that the FeO/SiO<sub>2</sub> ratio influences the mineralogical phase distribution.

#### 3.2.1. Laboratory Scale

The back scattered electron (BSE) images of the original sample A and the remelted sample AR2 (moderate cooling, laboratory scale) in Figure 3a,b show that remelting the slag without quartz addition already had an effect on the mineralogical phase distribution. The spinel grain size increased from



approximately 10  $\mu\text{m}$  to approximately 100  $\mu\text{m}$ , the dendritic wuestite shape was more dominant than the spherical shape, and instead of olivine, bredigite ( $\text{Ca}_7\text{Mg}(\text{SiO}_4)_4$ ) was formed. Nevertheless, the abundance of calcium silicate phases was still low. A comparison of the different cooling rates revealed that the size of the mineral phases, especially the spinel size, increased with decreasing cooling rate (see Supplementary Materials Figure S1). A possible explanation for the higher abundance of spinel phases compared to the original sample due to solely remelting the material might be an interaction between the crucible material and the melt, since MgO is known to foster spinel formation [5,29]. However, chemical analyses (Table 1, Section 3.3) showed that the material input (MgO) for the remelted slag samples was not significant. Quantitative EMP analyses performed on individual spinel grains (see Supplementary Materials Tables S2–S21) showed that the MgO concentrations per phase were comparable for the original sample A ( $11.1 \pm 0.53$  mass-%) and the samples AR1–3 ( $11.8 \pm 1.5$  mass-%,  $14.1 \pm 0.58$  mass-%, and  $12.5 \pm 1.2$  mass-%, respectively). Additionally, EMP analyses revealed that fast cooling led to an inhomogeneous distribution of FeO (24.2–63.0 mass-%) and  $\text{Cr}_2\text{O}_3$  (0.36–39.8 mass-%) in spinel, resulting in either Fe-rich or Cr-rich spinel phases. However, the sum of FeO and  $\text{Cr}_2\text{O}_3$  concentrations was rather constant ( $62.6 \pm 1.9$  mass-%). In contrast, the FeO and  $\text{Cr}_2\text{O}_3$  concentrations measured in spinel phases in sample AR2 (moderate cooling) and in the original sample A were rather homogenous within the range of standard deviations of the performed EMP analyses ( $30.0 \pm 3.0$  mass-% and  $30.8 \pm 1.8$  mass-% for sample A, respectively,  $38.5 \pm 3.0$  mass-% and  $23.7 \pm 1.6$  mass-% for sample AR2). The increased abundance of larger spinels in sample AR3 (slow cooling) led to reduced  $\text{Cr}_2\text{O}_3$  concentrations of 0.32–8.1 mass-% per analyzed phase, but to increased FeO concentrations of 45.9–56.1 mass-%. The sum of FeO and  $\text{Cr}_2\text{O}_3$  was again quite homogeneous with  $54.4 \pm 2.7$  mass-%. In contrast to the original sample A, V was only in few spinel analyses above the detection limit of the applied method with concentrations ranging from 0.05 mass-% to 0.08 mass-%. The same applied to V in the measured wuestite solid solutions (0.06–0.07 mass-% V), however, in all measured phases, Cr was detected with concentrations of  $0.6 \pm 0.1$  mass-% to  $1.1 \pm 0.3$  mass-%. Quantitative analyses on calcium silicate phases was only possible in sample AR3, since the two phases identified in samples AR1 and AR2 were too small and no discrete grain boundaries were found. For sample AR3, XRD analyses (Figure S2) confirmed the formation of bredigite, but the Al-bearing calcium silicate phase could not be unequivocally assigned to melilite or pyroxene by XRD or EMP analyses. In all remelted samples, neither Cr nor V were detected in the measured calcium silicate phases via EMP analyses.

The addition of quartz sand (sample AC2, Figure 3c) significantly changed the mineral phase proportions by increasing the calcium silicate and spinel formation and repressing the wuestite crystallization. In addition, the mineralogical composition (determined by XRD and, if possible, quantitative EMP analyses (Figure S2 and Tables S2–S21)) changed, because pyroxene formed instead of melilite. According to the FactSage<sup>TM</sup> calculations, the formation of pyroxene indicates that slightly more  $\text{SiO}_2$  was added during the experiments than intended. Quantitative EMP analyses on spinel phases revealed that instead of a Cr/Fe spinel with an Al-rim (original sample, Figure 3a), Fe-rich, or zoned Cr-rich spinels with a Fe-rim were formed (sample AC2, Figure 3c). This is in accordance with Qichen et al. (1997) [30], showing that the high FeO concentrations available in the melt were consumed by spinel, olivine, and pyroxene instead of wuestite, resulting in Fe-rich and Mg-poor rims in spinel and Fe-poor and Mg-rich neighboring mineral phases (e.g., olivine) due to intergrain ion exchange, which is induced by temperature changes.

Similar to the remelted slag samples, V was only detected in some spinel phases, but with concentrations from 0.06 mass-% up to 0.1 mass-%. The incorporation of V in a lower amount of spinel phases compared to the original samples (Table S2–S21) was consistent with the increased spinel formation, as the  $\text{V}_2\text{O}_3$  concentrations in the melt were identical to the original sample A. EMP analyses performed on calcium silicate phases showed that, aside from pyroxene, two types of olivine, rich in Ca or Mg, were formed (Figure 3c). Chromium and V were detected in some measured grains of the Mg-rich olivine, but neither in the Ca-rich olivine (except for sample AC1) nor in pyroxene.

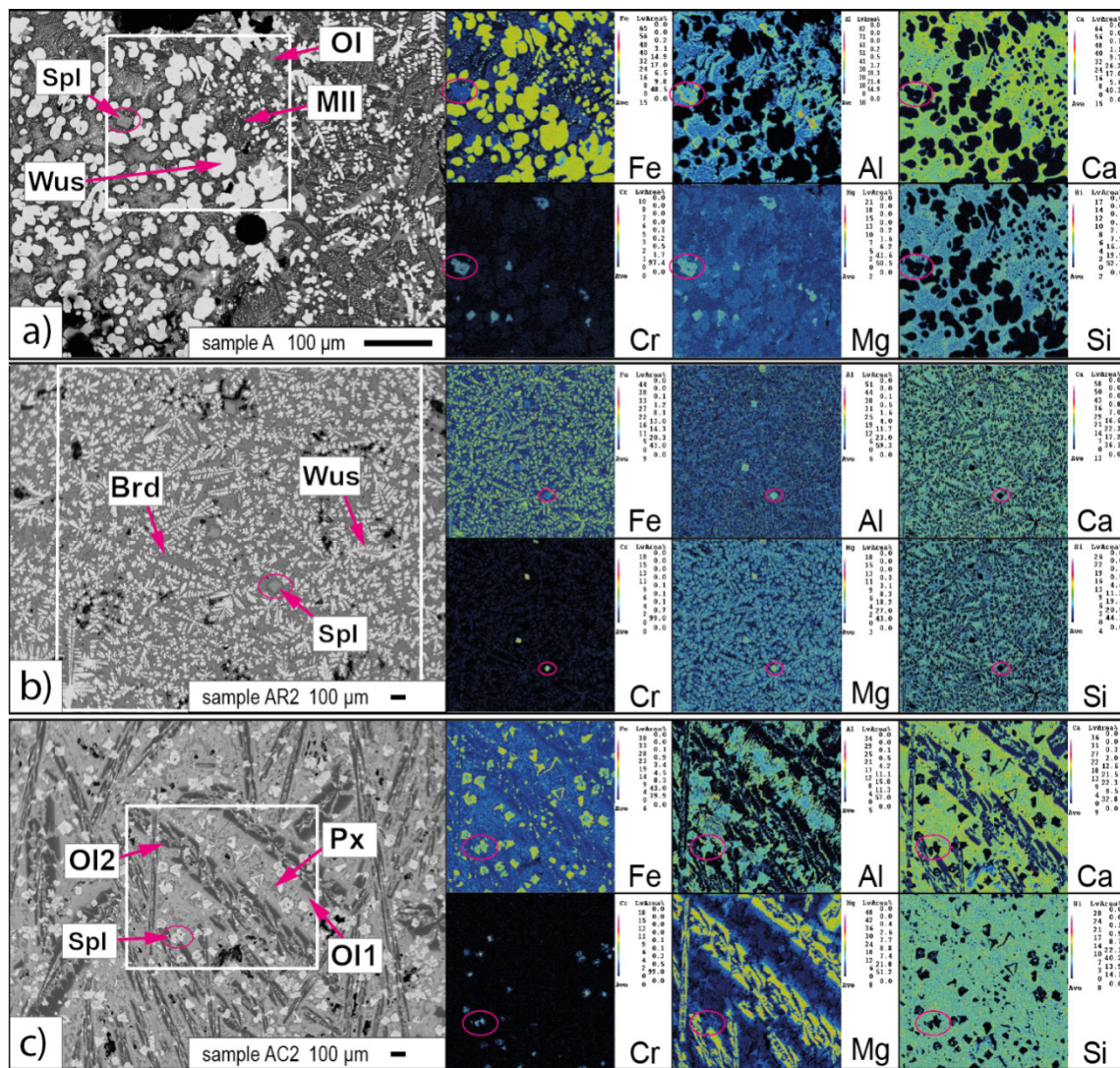


**Figure 3.** Back scattered electron (BSE) images and element mappings (Fe, Al, Ca, Cr, Mg, Si) of samples derived from the laboratory experiments: (a) sample A, (b) remelted sample AR2 (moderate cooling) and (c) conditioned sample AC2 (moderate cooling). Circles mark the element distribution in the spinel phase as an example. Abbreviations according to Whitney and Evans (2010) [28]: wuestite solid solution (Wus), spinel solid solution (Spl), olivine group phase (Ol), melilite group phase (Mll), bredigite (Brd), Ca-rich olivine (Ol1), Mg-rich olivine (Ol2), and pyroxene (Px). Phases identified via x-ray diffraction (XRD) and, if possible, via quantitative electron microprobe (EMP) analyses.

### 3.2.2. Pilot Plant Scale

Figure 4 shows secondary electron (SE) images of the samples BR1–3 and BC1–3 as well as of the original sample B from the pilot scale experiments. The higher CaO input provided in the steel plant during the formation process of slag sample B led to the appearance of different calcium (silicate) phases compared to sample A: instead of olivine phases, larnite (determined via XRD, Figure S2) was formed and brownmillerite occurred instead of melilite. Although the polished sections used for the EMP analyses were prepared without water, larnite was removed on the surface of the original sample B and the remelted samples BR1–3.



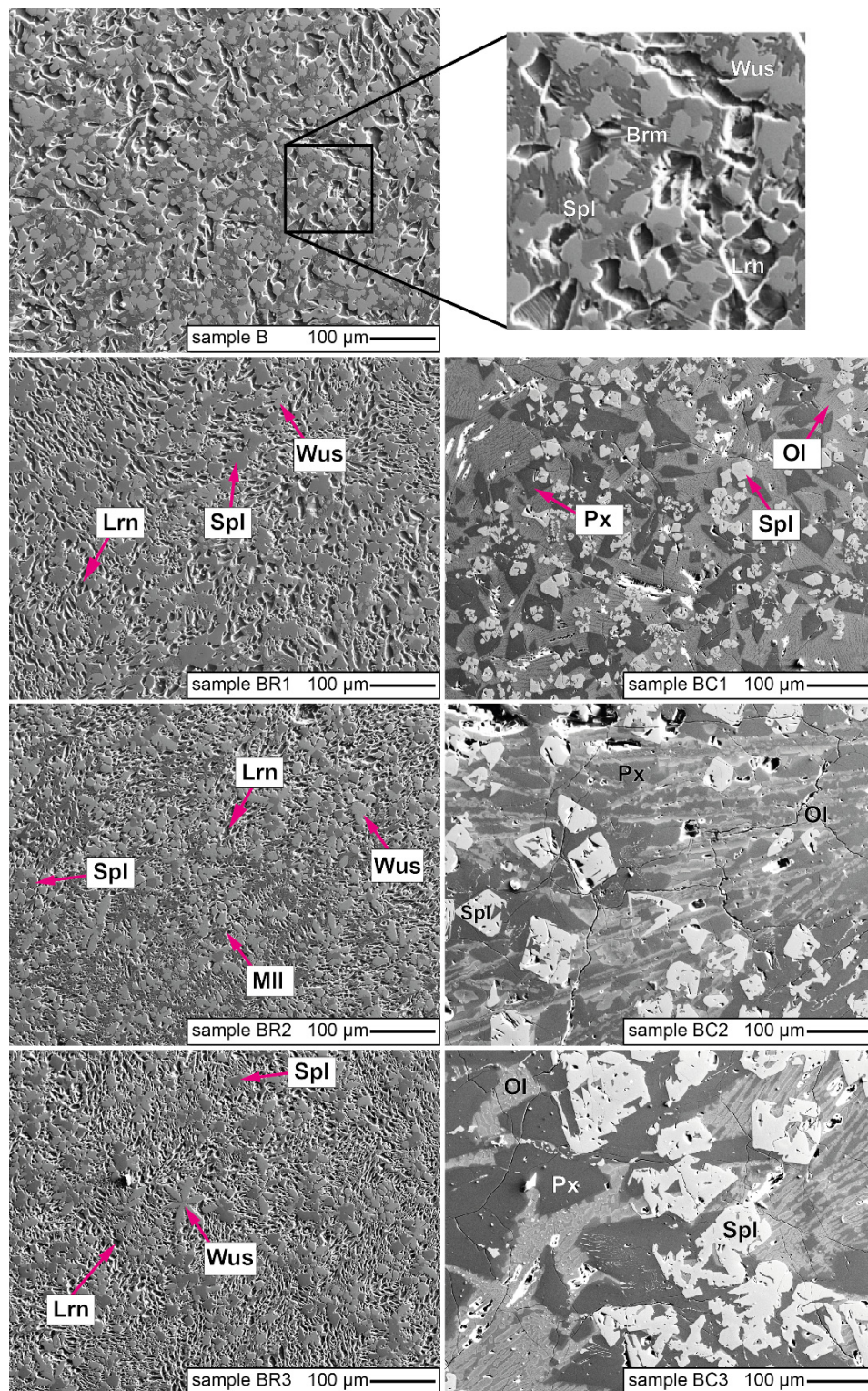


**Figure 4.** Secondary electron (SE) images of original sample B, remelted samples BR1–3, and remelted conditioned samples BC1–3 from pilot scale experiments. Numbers 1–3 represent different cooling rates with (1) fast cooling, (2) moderate cooling, and (3) slow cooling. Abbreviations according to Whitney and Evans (2010) [28]: wuestite solid solution (Wus), spinel solid solution (Spl), larnite (Lrn), olivine group (Ol), and melilite group (Mll). Phases identified via x-ray diffraction (XRD) and, if possible, via quantitative electron microprobe (EMP) analyses.

As with sample A (Figure 3), the remelting of sample B had an effect on the spinel size and abundance, but not on the overall mineral phase composition. However, the quartz sand addition did have several effects: no wuestite was formed and the crystallization of calcium silicate phases such as olivine and pyroxene, which are less soluble phases compared to larnite, was enhanced. The appearance of pyroxene indicates that the SiO<sub>2</sub> content in the slag was slightly higher than that calculated during the experiments. The size of the mineral phases in the remelted samples BR1–3 was not as strongly affected by the cooling rate as in the laboratory experiments, but the influence of the cooling rate was significant for all phases in the conditioned samples BC1–3 (Figure 4).

Quantitative EMP analyses (Table S2–S21) were only possible for spinel and wuestite in samples BR1–3 because larnite was removed during the preparation, and for spinel and pyroxene in samples BC1–3 because the acicular olivine crystals were too thin for quantitative analysis. Fe-rich and Cr-rich spinels were present in all samples derived from the pilot scale experiments, but in contrast to the laboratory experiments, the sum of Cr<sub>2</sub>O<sub>3</sub> and FeO was less homogeneously distributed in the remelted samples (samples BR1–3). The Fe and Cr zonation was clearly visible in the recorded element mappings of, for example, sample BC3 (Figure S3). The change in spinel shape in the conditioned samples may indicate changes in the local activities of oxygen and deoxidation metals (e.g., Mn) as well as varying solidification conditions. Similar shapes were described by Steinmetz and Lindenberg (1976) [31] for Fe–Mn–O and Fe–Si–O equilibrium systems with Cr. In all samples, V was detected in hardly any measured spinels, but, if detected, with concentrations ranging from 0.1 mass-% up to 0.6 mass-% (for comparison original sample B: 0.1–0.2 mass-% V). In all measured wuestite phases of samples BR1–3, Cr was detected ( $0.07 \pm 0.04$  mass-% to  $0.4 \pm 0.07$  mass-%) and in few grains V (0.3–0.6 mass-%). No general conclusion can be drawn for the investigated pyroxene phases of samples BC1–3, since Cr and V were only present in a limited amount of measured phases and in concentrations slightly above the detection limit (Table S2–S21).

### 3.2.3. Collective Mineralogical Results

The EMP analyses performed on spinel grains indicate that in most samples derived from the laboratory and pilot scale experiments, an oxidation, especially of iron, was not completely suppressed, although a nitrogen atmosphere and/or iron filings were provided, because the total values were below 100% (Tables S2–S22).

Neither in the laboratory nor in the pilot scale experiments were glassy SiO<sub>2</sub> phases found, although the relatively high SiO<sub>2</sub> input changed the basicity to very low values of 0.57–0.69 (Table 1, Section 3.3) and some samples were cooled rapidly. It was assumed that the high Al<sub>2</sub>O<sub>3</sub> and CaO concentrations (Table 1, Section 3.3) in the original samples A and B prohibit a glass phase formation as stated by Lindvall et al. (2017) [32].

Based on the performed experiments, the driving force for the enhanced spinel formation could not be distinctly identified. It could not be confirmed that the formation of magnesiowuestite indirectly prohibits the spinel formation [9] by withdrawing MgO, which fosters spinel formation [5,29] from the melt. Spinel formation was increased in all samples: the remelted samples with high magnesiowuestite abundance and the conditioned samples with hardly any magnesiowuestite formation. Additionally, the influence of the crucible and refractory material could not be identified as the driving force for the increased spinel formation in all samples. Furthermore, after the quartz sand addition in the laboratory scale, silicate phases with up to 40 mass-% MgO were formed, suggesting that most of the available MgO was consumed by the silicate phases and not by the spinel phase. Although the performed FactSage<sup>TM</sup> calculations (Figure 1a–c, Section 3.1) suggested that spinels were formed before calcium silicate phases, especially olivine, the fractional crystallization theory and investigations on igneous rocks [18,33–35] postulate that spinel and olivine crystallize together, which also explains the observed zoning in spinel grains (see above). No Mg-rich olivine phase was found in the pilot scale experiments. The MgO inclusions with a diameter of several 100 µm, seen in the rapidly cooled conditioned sample BC1 (Figure S4), are most likely due to parts of the damaged refractory material. In general, it is



assumed that the cooling rate, the oxygen fugacity, and the decrease in viscosity [36] has a higher impact on spinel formation than the MgO concentrations in the molten slag.

### 3.3. Chemical Analyses and Leaching Results

As intended, the FeO/SiO<sub>2</sub> ratio decreased with the quartz addition from above three to almost one in both experiments, being in good agreement with the calculated ratios via FactSage™ (1.12 and 1.06). In the pilot scale experiments, the FeO/SiO<sub>2</sub> ratio increased for the remelted slag samples from above three to above four (Table 1). The CaO/SiO<sub>2</sub> ratio also decreased significantly, resulting in a more acidic melt and a higher MgO input from the crucible and refractory material compared to the remelted samples. The basicity achieved experimentally was also in good agreement with the calculated ratios by FactSage™ (0.62 and 0.74).

The remelting and the targeted modification during the remelting had a significant influence on the amount of Cr and V leached from the slag (Table 1 and Figure 5) in both the laboratory and pilot scale experiments. Due to the small sample size (approximately 260 g) derived from the laboratory experiments, only leaching tests with distilled water (natural pH) were conducted (Table 1). The samples derived from the pilot scale experiments (10–20 kg per sample) were investigated over the pH range from 2–14 (Figure 5). The leaching experiments are described in detail in Section 2.4. The leached amounts of Cr and V at natural pH as well as the total content of MgO, Al<sub>2</sub>O<sub>3</sub>, V<sub>2</sub>O<sub>5</sub>, and Cr<sub>2</sub>O<sub>3</sub> in the solid samples and the FeO/SiO<sub>2</sub>, respectively, the CaO/SiO<sub>2</sub> ratios are given in Table 1. The complete chemical characterization of the original samples A, B and C is provided in Table S23. In order to compensate for differences in chemical composition caused by crucible and refractory material interactions during the experiments or by the dilution of the melt, the leached amount is discussed as % of the total content.

The original sample A showed elevated leaching for V and Cr compared to sample C (Table 1). Remelting the slags already decreased Cr and V concentrations in the leachate from  $1.1 \times 10^{-03}\%$  of the total Cr content to  $9.0 \times 10^{-06}\%$  of the total Cr content, and from 0.34% of the total V content to 0.07% of the total V content after the conducted laboratory experiments. The quartz sand addition lowered the leaching of V even further to 0.01% of the total V content, and therefore led to absolute leaching values of 10 to 100 times below the limit value for the use of recycling building materials (1.0 mg/kg DM) in Austria [14]. Chromium leaching after the modification was comparable to leaching after the remelting experiments.

The higher CaO input during the formation of original sample B led to the formation of larnite. According to Hobson et al. (2017) [7], V is released during the dissolution of larnite, but may be incorporated in newly formed calcium silicate hydrates. This is supported by the fact that the V leaching from sample B at natural pH (with distilled water) was already lower than for original samples A and C (Table 1). However, the conducted pH dependence leaching tests (Figure 5) revealed that this was only valid for leaching with distilled water. A low release of V throughout the pH range from 8 to 12 was only achieved for the modified samples and original sample C, which were characterized by low wuestite and high spinel abundance as well as high calcium silicate phase formation such as melilite and olivine (with low solubility), but no larnite (with high solubility). The V release from the original sample A, but even more significantly from original sample B, increased below pH 11. This led to the assumption that during aging and carbonation of the slag samples, which leads to a pH decrease of the leachates [37,38], more V was leached from the original sample compared to the conditioned slag samples. The formation of less soluble calcium silicate phases due to the quartz sand addition is represented by the pH-dependent release of Ca and Si (Figure 5). Previous studies on EAF slags [9] and converter slags from the basic oxygen steelmaking process [7,8,39] showed that larnite/dicalcium silicate may contain V and that this phase is highly soluble. Therefore, a modification to less soluble Fe bearing olivine, melilite, and pyroxene phases due to an increased SiO<sub>2</sub> concentration in the molten slag additionally minimizes V leaching. The remelted slag samples BR1–3 released more V during the performed pH dependence leaching tests than the original sample B, which is in accordance with the



increased FeO/SiO<sub>2</sub> ratio of above four after the experiments (Figure 5 and Table 1). For Cr, the pure remelting of sample B had a greater effect than the combined remelting and SiO<sub>2</sub> addition. However, all modified samples met the limit value for Cr, according to the recycling building materials ordinance in Austria (0.3 mg/kg DM; [14]).

The melting experiments and the performed leaching tests illustrate that the leaching behavior of V and Cr does not correlate with the total content in the slag, but is controlled by the mineralogical binding of the elements. This becomes evident because, despite the high total contents of Cr (up to 3 mass-%), only a small proportion of Cr is released during leaching with distilled water; whereas comparatively high amounts of V are released, although the total concentration of V is about 0.1 mass-%. In addition, the leaching behavior was improved by changing the mineral phase composition and distribution (e.g., formation of less soluble calcium silicate phases) in the modified slag samples.

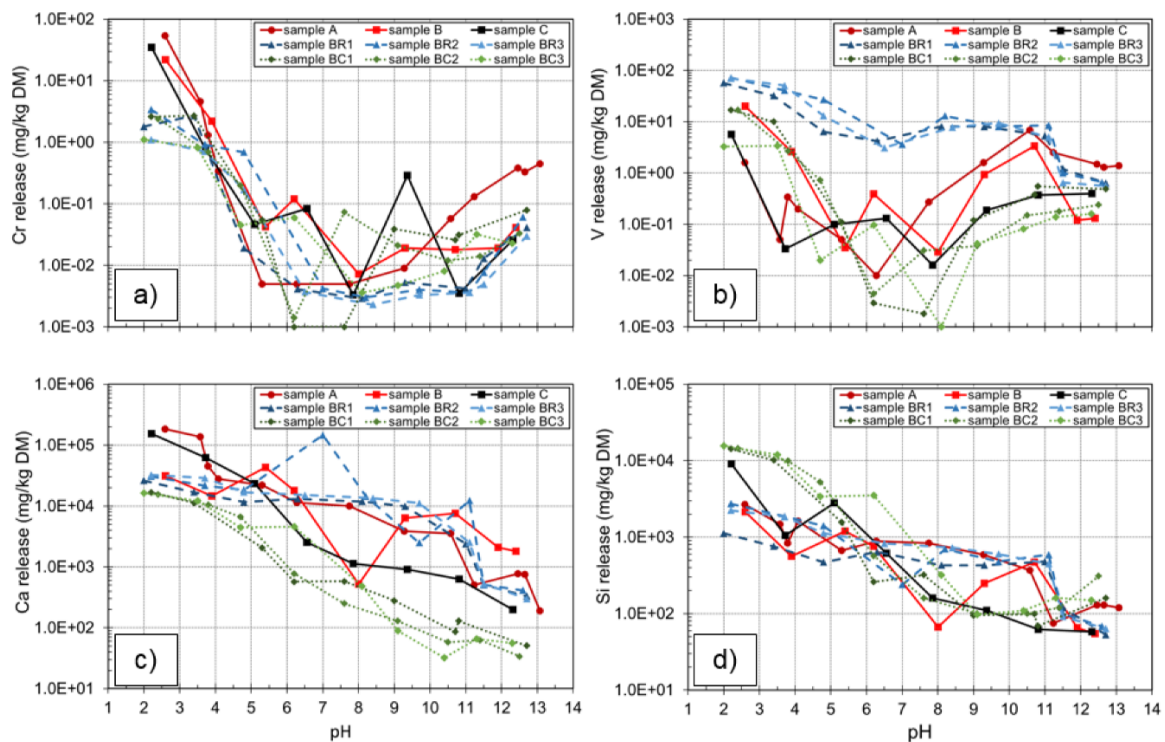


**Figure 5.** pH-dependent leaching behavior. (a) Cr, (b) V, (c) Ca, and (d) Si for original samples A, B, C and remelted samples BR1–3 as well as for remelted and modified samples BC1–3.

**Table 1.** Leached concentrations of V and Cr at natural pH (shaken with distilled water) for original samples A, B, and C as well as for remelted samples AR1–3 and BR1–3 and remelted, modified samples AC1–3 and BC1–3. Total concentrations of  $\text{Cr}_2\text{O}_3$ ,  $\text{V}_2\text{O}_3$ ,  $\text{MgO}$ , and  $\text{Al}_2\text{O}_3$  as well as ratios of  $\text{FeO}/\text{SiO}_2$  and  $\text{CaO}/\text{SiO}_2$ .

| Sample | pH   | Leached Concentrations with Distilled Water |      |            |       | Total Concentrations    |                        |      |                         |                           |                           |
|--------|------|---|------|------------|-------|-------------------------|------------------------|------|-------------------------|---------------------------|---------------------------|
|        |      | [% of Total Content]                        |      | [mg/kg DM] |       | [mass-%]                |                        |      |                         | Ratio                     |                           |
|        |      | Cr  | V    | Cr         | V     | $\text{Cr}_2\text{O}_3$ | $\text{V}_2\text{O}_3$ | MgO  | $\text{Al}_2\text{O}_3$ | $\text{FeO}/\text{SiO}_2$ | $\text{CaO}/\text{SiO}_2$ |
| A      | 11.2 | $1.1 \times 10^{-03}$                       | 0.34 | 0.13       | 2.5   | 1.73                    | 0.11                   | 6.20 | 7.28                    | 3.66                      | 2.03                      |
| AR1    | 11.0 | $6.4 \times 10^{-04}$                       | 0.19 | 0.076      | 1.2   | 1.72                    | 0.09                   | 6.53 | 8.26                    | 3.26                      | 1.54                      |
| AR2    | 10.8 | $2.9 \times 10^{-05}$                       | 0.06 | 0.0024     | 0.37  | 1.20                    | 0.08                   | 6.45 | 7.58                    | 3.35                      | 1.89                      |
| AR3    | 10.9 | $9.0 \times 10^{-06}$                       | 0.07 | 0.0018     | 0.38  | 2.98                    | 0.08                   | 7.23 | 7.18                    | 3.83                      | 1.59                      |
| AC1    | 10.1 | $8.8 \times 10^{-04}$                       | 0.03 | 0.046      | 0.13  | 0.76                    | 0.06                   | 13.9 | 6.61                    | 1.12                      | 0.57                      |
| AC2    | 10.0 | $6.0 \times 10^{-05}$                       | 0.01 | 0.0043     | 0.019 | 1.03                    | 0.05                   | 12.6 | 6.73                    | 1.21                      | 0.60                      |
| AC3    | 10.1 | $6.7 \times 10^{-05}$                       | 0.01 | 0.0024     | 0.025 | 0.52                    | 0.05                   | 13.1 | 6.48                    | 1.05                      | 0.57                      |
| B      | 11.9 | $1.5 \times 10^{-04}$                       | 0.02 | 0.019      | 0.12  | 1.86                    | 0.11                   | 3.47 | 9.58                    | 3.42                      | 2.38                      |
| BR1    | 11.5 | $1.1 \times 10^{-04}$                       | 0.19 | 0.013      | 1.2   | 1.81                    | 0.09                   | 3.79 | 8.35                    | 4.71                      | 2.54                      |
| BR2    | 11.5 | $5.7 \times 10^{-05}$                       | 0.17 | 0.0077     | 1.0   | 1.97                    | 0.09                   | 3.82 | 8.67                    | 4.76                      | 2.62                      |
| BR3    | 11.5 | $3.5 \times 10^{-04}$                       | 0.11 | 0.0049     | 0.65  | 0.20                    | 0.09                   | 3.82 | 9.24                    | 4.80                      | 2.65                      |
| BC1    | 10.7 | $2.6 \times 10^{-04}$                       | 0.09 | 0.026      | 0.38  | 1.45                    | 0.06                   | 7.13 | 7.14                    | 1.24                      | 0.69                      |
| BC2    | 10.5 | $1.3 \times 10^{-04}$                       | 0.04 | 0.012      | 0.15  | 1.36                    | 0.06                   | 8.42 | 6.80                    | 1.20                      | 0.65                      |
| BC3    | 10.4 | $9.2 \times 10^{-05}$                       | 0.02 | 0.0081     | 0.081 | 1.29                    | 0.06                   | 8.07 | 6.78                    | 1.25                      | 0.65                      |
| C      | 10.8 | $2.4 \times 10^{-05}$                       | 0.03 | 0.0035     | 0.37  | 2.13                    | 0.16                   | 3.92 | 9.13                    | 1.04                      | 0.94                      |

#### 4. Conclusions

The conducted experiments presented in this study support the hypothesis that the release of Cr and especially V can be minimized by decreasing the FeO/SiO<sub>2</sub> ratio in EAF slags. In contrast to the original sample, the leached V concentrations of the samples modified with quartz sand were 10 to 100 times below the limit value for the use of recycling building materials in Austria. Although the original samples already showed leachate concentrations of Cr below the limit values in Austria, Cr leaching was reduced even further in some samples, which is promising for possibly stricter limit values in future. Furthermore, the experiments provided information on the influence of the chemical composition of the melt and the cooling rate on spinel formation and the associated Cr leaching. By adding quartz sand to the molten slag, the wuestite formation was suppressed and the formation of spinel, which is characterized by a lower solubility, fostered. Additionally, a transformation from highly soluble larnite to less soluble calcium silicate phases was achieved. Both effects led to a decrease in V and Cr leaching at natural pH compared to the original samples in the laboratory experiments. Investigation of the pH-dependent leaching behavior of the samples derived from pilot scale experiments demonstrated that the release of V was minimized over a pH range from 8 to 12. The performed FactSage<sup>TM</sup> calculations were in good agreement with the obtained experimental data and served as a basis for the melting experiments. The described up scaling from the laboratory scale to the pilot plant scale was also successful. However, since the presented results showed preliminary results on two EAF slags only, the experiments need to be repeated for further up scaling with a statistically more significant number of samples. Further research will also consider how the economic and ecologic feasibility can be improved by reducing the amount of quartz sand or replacing it with alternative materials as the source of SiO<sub>2</sub> (e.g., residuals from the recycling of building materials).

**Supplementary Materials:** The following are available online at <http://www.mdpi.com/2076-3417/10/7/2549/s1>, Table S1: Input data and selected base phases with end members for the performed FactSage<sup>TM</sup> calculations; Tables S2–S22: Results of the performed chemical mineral EMPA analyses; Table S23: Chemical composition of original samples A, B and C; Figure S1: BSE images and element mappings of samples derived from the laboratory experiments; Figure S2: XRD patterns of all described samples; Figure S3: BSE image and element mapping of sample BC3; Figure S4: BSE images of MgO inclusions and EDS analyses for sample BC1.

**Author Contributions:** Conceptualization, S.N., D.A., P.D., B.A., P.P., K.P.S., J.S., J.G.R., R.P., and D.V.; Methodology, S.N., D.A., P.D., B.A., P.P., K.P.S., J.S., J.G.R., R.P., and D.V.; Software, S.N., P.P., and J.S.; Investigation, S.N., D.A., P.D., B.A., and D.V.; Resources, D.A., P.D., B.A., P.P., J.S., and J.G.R.; Writing—original draft preparation, S.N.; Writing—review and editing, S.N., D.A., P.D., B.A., P.P., K.P.S., J.S., J.G.R., R.P., and D.V.; Visualization, S.N. and K.P.S.; Supervision, S.N., J.G.R., R.P., and D.V.; Project administration, S.N. and D.V.; Funding acquisition, R.P. and D.V. All authors have read and agreed to the published version of the manuscript.

**Funding:** This research was funded by the Austrian Research Promotion Agency (FFG) (grant number 851210, program “Bridge Early Stage”, project MiLeSlag (Mineralogy and Leachability of Steel Slags)).

**Acknowledgments:** The authors thank all participating project partners, Chair of Resource Mineralogy, Chair of Ferrous Metallurgy, Federal Institute for Materials Research and Testing, FEhS Building Materials Institute, ECN part of TNO, Max Aicher Umwelt GmbH, PORR Umwelttechnik GmbH, Scholz Austria GmbH and Stahl- und Walzwerk Marienhütte GmbH for their contributions throughout the project. Special thanks go to the laboratory staff and colleagues at the Chair of Waste Processing Technology and Waste Management, to Federica Zaccarini and Maik Zimmermann (both Chair of Resource Mineralogy) for the sample preparation and the support with the electron microprobe analyses, and to Rolf Kobs and Gerhard Kindler (both FEhS) as well as to Adib Hanna and Dirk Stolle (both BAM) for their commitment during the melting experiments.

**Conflicts of Interest:** The authors declare no conflicts of interest.

#### References

1. Aldrian, A.; Raith, J.G.; Höllen, D.; Pomberger, R. Influence of Chromium Containing Spinel in an Electric Arc Furnace Slag on the Leaching Behaviour. *J. Solid Waste Technol. Manag.* **2015**, *41*, 357–365. [CrossRef]
2. Mudersbach, D.; Kuehn, M.; Geiseler, J.; Koch, K. Chromium Immobilisation in EAF-Slags from High-alloy Steelmaking: Tests at FEhS-Institute and Development of an Operational Slag Treatment Process. In *Proceedings of the First Slag Valorisation Symposium*; KU Leuven: Leuven, Belgium, 2009; pp. 101–110.

3. Strandkvist, I.; Engström, F.; Pålsson, K.; Björkman, B. The Influence of Iron Oxide on the Chromium Leachability of EAF Slag—A Full-Scale Study At Ovako Hofors. In Proceedings of the Scanmet IV: 4th International Conference on Process Development in Iron and Steelmaking, Luleå, Sweden, 10–13 June 2012; pp. 329–338.
4. Mombelli, D.; Mapelli, C.; Barella, S.; Di Cecca, C.; Le Saout, G.; Garcia-Diaz, E. The effect of chemical composition on the leaching behaviour of electric arc furnace (EAF) carbon steel slag during a standard leaching test. *J. Environ. Chem. Eng.* **2016**, *4*, 1050–1060. [[CrossRef](#)]
5. Cabrera-Real, H.; Romero-Serrano, A.; Zeifert, B.; Hernandez-Ramirez, A.; Hallen-Lopez, M.; Cruz-Ramirez, A. Effect of MgO and CaO/SiO<sub>2</sub> on the immobilization of chromium in synthetic slags. *J. Mater. Cycles Waste Manag.* **2012**, *14*, 317–324. [[CrossRef](#)]
6. Lončnar, M.; van der Sloot, H.A.; Mladenović, A.; Zupančič, M.; Kobal, L.; Bukovec, P. Study of the leaching behaviour of ladle slags by means of leaching tests combined with geochemical modelling and mineralogical investigations. *J. Hazard. Mater.* **2016**, *317*, 147–157. [[CrossRef](#)]
7. Hobson, A.J.; Stewart, D.I.; Bray, A.W.; Mortimer, R.J.G.; Mayes, W.M.; Rogerson, M.; Burke, I.T. Mechanism of Vanadium Leaching during Surface Weathering of Basic Oxygen Furnace Steel Slag Blocks: A Microfocus X-ray Absorption Spectroscopy and Electron Microscopy Study. *Environ. Sci. Technol.* **2017**, *51*, 7823–7830. [[CrossRef](#)]
8. van Zomeren, A.; van der Laan, S.R.; Kobesen, H.B.A.; Huijgen, W.J.J.; Comans, R.N.J. Changes in mineralogical and leaching properties of converter steel slag resulting from accelerated carbonation at low CO<sub>2</sub> pressure. *Waste Manag.* **2011**, *31*, 2236–2244. [[CrossRef](#)]
9. Neuhold, S.; van Zomeren, A.; Dijkstra, J.J.; van der Sloot, H.A.; Drissen, P.; Algermissen, D.; Mudersbach, D.; Schüler, S.; Griessacher, T.; Raith, J.G.; et al. Investigation of Possible Leaching Control Mechanisms for Chromium and Vanadium in Electric Arc Furnace (EAF) Slags Using Combined Experimental and Modeling Approaches. *Minerals* **2019**, *9*, 525. [[CrossRef](#)]
10. Dimitrova, S.V.; Mihailova, I.K.; Nikolov, V.S.; Mehendjiev, D.R. Adsorption capacity of modified metallurgical slags. *Bulg. Chem. Commun.* **2012**, *44*, 30–36.
11. Pasetto, M.; Baldo, N. Mix design and performance analysis of asphalt concretes with electric arc furnace slag. *Constr. Build. Mater.* **2011**, *25*, 3458–3468. [[CrossRef](#)]
12. Faleschini, F.; Brunelli, K.; Zanini, M.A.; Dabalà, M.; Pellegrino, C. Electric Arc Furnace Slag as Coarse Recycled Aggregate for Concrete Production. *J. Sustain. Metall.* **2016**, *2*, 44–50. [[CrossRef](#)]
13. Sas, W.; Głuchowski, A.; Radziemska, M.; Dzieciotł, J.; Szymański, A. Environmental and Geotechnical Assessment of the Steel Slags as a Material for Road Structure. *Materials* **2015**, *8*, 4857–4875. [[CrossRef](#)]
14. Bundesministerium für Land- und Forstwirtschaft, Umwelt und Wasserwirtschaft. *Verordnung des Bundesministers für Land- und Forstwirtschaft, Umwelt und Wasserwirtschaft über die Pflichten bei Bau- oder Abbruchtätigkeiten, die Trennung und die Behandlung von bei Bau- oder Abbruchtätigkeiten anfallenden Abfällen, die Herstellung und das Abfallende von Recycling-Baustoffen (Recycling-Baustoffverordnung—RBV)*; Bundesministerium für Land- und Forstwirtschaft, Umwelt und Wasserwirtschaft: Vienna, Austria, 2016; p. 162.
15. Jellinghaus, M. *Stahlerzeugung im Lichtbogenofen*; 3. Auflage.; Stahleisen: Düsseldorf, Germany, 1994; ISBN 3514005028.
16. Liu, Z.; Pandelaers, L.; Jones, P.T.; Blanpain, B.; Guo, M. Effect of Al<sub>2</sub>O<sub>3</sub> and SiO<sub>2</sub> Addition on the Viscosity of BOF Slag. In *Advances in Molten Slags, Fluxes, and Salts: Proceedings of the 10th International Conference on Molten Slags, Fluxes and Salts 2016*; Springer International Publishing: Cham, Switzerland, 2016; pp. 439–446.
17. Drissen, P. *Eisenhüttenschlacken—Industrielle Gesteine*; Report des FEhS-Instituts für Baustoff-Forschung e.V.: Duisburg, Germany, 2004.
18. Bowen, N.L. *The Evolution of Igneous Rocks*; Princeton University Press: Princeton, NJ, USA, 1928; ISBN 978-0486603117.
19. Tossavainen, M.; Engstrom, F.; Yang, Q.; Menad, N.; Lidstrom Larsson, M.; Bjorkman, B. Characteristics of steel slag under different cooling conditions. *Waste Manag.* **2007**, *27*, 1335–1344. [[CrossRef](#)]
20. Mombelli, D.; Mapelli, C.; Barella, S.; Gruttadauria, A.; Le Saout, G.; Garcia-Diaz, E. The efficiency of quartz addition on electric arc furnace (EAF) carbon steel slag stability. *J. Hazard. Mater.* **2014**, *279*, 586–596. [[CrossRef](#)]
21. Austrian Standards Institute. *ÖNORM S 2127:2011 Grundlegende Charakterisierung von Abfallhaufen oder von festen Abfällen aus Behältnissen und Transportfahrzeugen*; Austrian Standards Institute: Vienna, Austria, 2011.

22. Deutsches Institut für Normung. *DIN 19529 Elution von Feststoffen—Schüttelverfahren zur Untersuchung des Elutionsverhaltens von Anorganischen Stoffen mit einem Wasser/Feststoff-Verhältnis von 2 l/kg* 2009, 13; Deutsches Institut für Normung: Berlin, Germany, 2019.
23. Quarzwerke GmbH. *Leistungserklärung-Kennnummer 12620-2013-1* 2016, 5; Quarzwerke GmbH: Frechen, Germany, 2016.
24. Austrian Standards Institute. *ÖNORM EN 14346:2007 Charakterisierung von Abfällen—Berechnung der Trockenmasse durch Bestimmung des Trockenrückstandes oder des Wassergehaltes* 2007; Austrian Standards Institute: Vienna, Austria, 2007.
25. Austrian Standards Institute. *ÖNORM EN 13656:2002 Charakterisierung von Abfällen—Aufschluss mittels Mikrowellengerät mit einem Gemisch aus Fluorwasserstoffsäure (HF), Salpetersäure (HNO<sub>3</sub>) und Salzsäure (HCl) für die anschließende Bestimmung der Elemente im Abfall* 2002; Austrian Standards Institute: Vienna, Austria, 2002.
26. Austrian Standards Institute. *ÖNORM EN 14429:2015 Charakterisierung von Abfällen—Untersuchung des Elutionsverhaltens—Einfluss des pH-Wertes auf die Elution unter Vorheriger Säure/Base-Zugabe* 2015; Austrian Standards Institute: Vienna, Austria, 2015.
27. Austrian Standards Institute. *ÖNORM EN ISO 17294-2:2005 Wasserbeschaffenheit—Anwendung der Induktiv Gekoppelten Plasma-Massenspektrometrie (ICP-MS)* 2005; Austrian Standards Institute: Vienna, Austria, 2005.
28. Whitney, D.L.; Evans, B.W. Abbreviations for names of rock-forming minerals. *Am. Mineral.* **2010**, *95*, 185–187. [[CrossRef](#)]
29. White, J. The Relationship of Phase Diagrams to Constitution and Microstructure in Ceramic and Ceramic-Metal System. In *Refractory Materials A Series of Monographs*; Academic Press: New York, NY, USA; London, UK, 1970; Volume 6, pp. 21–66.
30. Qichen, F.; Ruoxin, L.; Zhuoran, L.; Hongshen, X.; Yuemin, Z. Experimental Research on Phase Transition of Al-rich Minerals in Upper Mantle of Eastern China and Its Significance. In *Proceedings of the 30th International Geological Congress*; VSP BV: Utrecht, The Netherlands; Tokyo, Japan, 1997; pp. 13–21.
31. Steinmetz, E.; Lindenberg, H.-U. Oxidmorphologie bei Mangan- und Mangan-Silicium-Desoxidation. In *Archiv für das Eisenhüttenwesen*; Verlag Stahleisen GmbH: Düsseldorf, Germany, 1976; Volume 47, pp. 71–76.
32. Lindvall, M.; Berg, M.; Sichen, D. The Effect of Al<sub>2</sub>O<sub>3</sub>, CaO and SiO<sub>2</sub> on the Phase Relationship in FeO–SiO<sub>2</sub> Based Slag with 20 Mass% Vanadium. *J. Sustain. Metall.* **2017**, *3*, 289–299. [[CrossRef](#)]
33. Thy, P. Spinel minerals in transitional and alkali basaltic glasses from Iceland. *Contrib. Mineral. Petrol.* **1983**, *83*, 141–149. [[CrossRef](#)]
34. Irvine, T.N. Chromian Spinel as a Petrogenetic Indicator: Part 1. Theory. *Can. J. Earth Sci.* **1965**, *2*, 648–672. [[CrossRef](#)]
35. Irvine, T.N. Chromian Spinel as a Petrogenetic Indicator: Part 2. Petrologic Applications. *Can. J. Earth Sci.* **1967**, *4*, 71–103. [[CrossRef](#)]
36. Li, J.L.; Xu, A.J.; He, D.F.; Yang, Q.X.; Tian, N.Y. Effect of FeO on the formation of spinel phases and chromium distribution in the CaO–SiO<sub>2</sub>–MgO–Al<sub>2</sub>O<sub>3</sub>–Cr<sub>2</sub>O<sub>3</sub> system. *Int. J. Miner. Metall. Mater.* **2013**, *20*, 253–258. [[CrossRef](#)]
37. Capobianco, O.; Costa, G.; Thuy, L.; Magliocco, E.; Hartog, N.; Baciocchi, R. Carbonation of stainless steel slag in the context of in situ Brownfield remediation. *Miner. Eng.* **2014**, *59*, 91–100. [[CrossRef](#)]
38. Huijgen, W.J.J.; Comans, R.N.J. Carbonation of Steel Slag for CO<sub>2</sub> Sequestration: Leaching of Products and Reaction Mechanisms. *Environ. Sci. Technol.* **2006**, *40*, 2790–2796. [[CrossRef](#)] [[PubMed](#)]
39. Drissen, P. *Mineralische Bindung von Spurenelementen in Stahlwerksschlacken*; Report des FEhS-Instituts für Baustoff-Forschung e.V.: Duisburg, Germany, 2006.

